A Simulation of Atmospheric Storm Tracks with a Forced Barotropic Model

SUKYOUNG LEE

Department of Meteorology, The Pennsylvania State University, University Park, Pennsylvania

JEFFREY L. ANDERSON

NOAA/Geophysical Fluid Dynamics Laboratory, Princeton University, Princeton, New Jersey

(Manuscript received 17 May 1995, in final form 30 November 1995)

ABSTRACT

A forced, nonlinear barotropic model on the sphere is shown to simulate some of the structure of the observed Northern Hemisphere midlatitude storm tracks with reasonable accuracy. For the parameter range chosen, the model has no unstable modes with significant amplitude in the storm track regions; however, several decaying modes with structures similar to the storm track are discovered. The model's midlatitude storm tracks also coincide with the location of a waveguide that is obtained by assuming that the horizontal variation of the time-mean flow is small compared with the scale of the transient eddies. Since the model is able to mimic the behavior of the observed storm tracks without any baroclinic dynamics, it is argued that the barotropic waveguide effects of the time-mean background flow acting on individual eddies are partially responsible for the observed storm track structure.

1. Introduction

Because of their importance in the general circulation, as well as their impact on local climate, midlatitude storm tracks have been a topic of active research in the past two decades. Much of this research has concentrated on trying to understand the zonally inhomogeneous structure of the storm tracks that occurs during the Northern Hemisphere (NH) winter. This has led to the theory of local baroclinic instability (Frederiksen 1983; Pierrehumbert 1984; Cai and Mak 1990), which argues that the two localized oceanic storm tracks form due to the existence of two regions of localized baroclinic instability. As a conceptual frame work, this theory has significantly contributed to our understanding of storm track dynamics.

Recently, attention has been drawn to the barotropic effects of the zonally varying background flow acting on the synoptic-scale storm track eddies. Using an idealized, linear barotropic model, Lee (1995) pointed out that a simple barotropic modulation of these synoptic-scale eddies by the background flow can also give rise to localized storm tracks. Whitaker and Dole (1995) demonstrated the effect of deformation on the localization of storm tracks in a two-layer model. Branstator (1995), employing a ray-tracing method, showed that synoptic-scale eddies can be strongly steered by larger-scale, low-frequency anomalies in a linearized version of the Community Climate Model.

This paper extends a hypothesis, advanced by Lee (1995) and Branstator (1995), that the distribution of extratropical transient eddy activity is largely determined by the barotropic steering of eddy activity by the time-averaged upper-tropospheric flow. This hypothesis is tested using a forced nonlinear barotropic model.

The experimental design is described in section 2. Section 3 presents model results and two paradigms for explaining the storm tracks in the barotropic model. Section 4 presents a number of additional sensitivity tests, while concluding remarks follow in section 5.

2. Experimental design

a. Forced barotropic model

In this study, a forced version of the barotropic vorticity equation (BVE) on the sphere,

$$\frac{\partial \nabla^2 \psi}{\partial t} + J(\psi, \nabla^2 \psi + f) + \kappa \nabla^{10} \psi = F, \quad (1)$$

is integrated using spherical harmonic basic functions. Unless otherwise specified, all experiments discussed are performed at a T42 truncation. In (1), ψ is the streamfunction, f is the Coriolis parameter, ∇^2 and J are the spherical Laplacian and Jacobian operators, and κ is the hyperviscosity coefficient. The forcing, F, is selected so that the time-mean streamfunction $\bar{\psi}$

Corresponding author address: Dr. Sukyoung Lee, Department of Meteorology, The Pennsylvania State University, 503 Walker Bldg., University Park, PA 16802-5013.
E-mail: sl@essc.psu.edu

of an extended integration of (1) will be similar to an observed climatology over the NH midlatitudes. In addition, the forcing must allow, if possible, for significant transient eddies with spatial and temporal scales similar to those found in observed midlatitude synoptic-scale eddies.

Here, these constraints are satisfied by strongly forcing large spatial scales toward an observed streamfunction climatology while allowing smaller spatial scales to evolve freely (Anderson 1995). Introducing this forcing in (1) and making explicit use of the representation as a sum of spherical harmonics gives

$$\frac{\partial \nabla^2 \psi}{\partial t} + J(\psi, \nabla^2 \psi + f) + \kappa \nabla^{10} \psi = \sum_{|m| \leq M} \sum_{|n| \leq N} \alpha(\psi_{m,n} - \psi^F_{m,n}) Y_{m,n}, \quad (2)$$

where α is the forcing strength; $\psi_{m,n}$ and $\psi^F_{m,n}$ are the spherical harmonic expansion coefficients of the streamfunction and the modified climatological forcing, respectively; and $Y_{m,n}$ is the spherical harmonic with total wavenumber n and zonal wavenumber m. This formulation of forcing was referred to as thermal forcing in Anderson (1995) since the right-hand side of (2) can be viewed as a thermal forcing in a shallow-water model context. Note that the forcing is only applied to a subset of the relatively large-scale spherical harmonic components limited by the value of N and M.

The hyperviscosity is included as a crude parameterization of the unresolved scales in the truncated model. The value of κ is defined in terms of the damping timescale associated with the smallest retained wave in the truncated model. For instance, a 1-day damping in a T42 model means that κ is selected so that the coefficients of waves with total wavenumber 42 will be damped with an e-folding time of 1 day.

b. *Forcing field*

The forcing field ψ^F in (2) is chosen as a modified version of an observed 300-mb monthly mean streamfunction field, ψ^{CDDB} from the Climate Diagnostic Data Base (CDDB) (Chelliah 1990). The observed monthly means are converted to the forcing fields by retaining only the zonal mean component of the observed field outside of the NH midlatitudes. This conversion is performed on the 33° latitude physical space Gaussian grid corresponding to a T21 truncated representation of the observed monthly mean. The observed zonally varying streamfunction is left unchanged in a band from approximately 20° to 60°N and changes from zonally varying to zonal mean over transition regions of approximately 20° latitude:

$$\psi^F_{ij} = \hat{\psi}^{\text{CDDB}}_j + \sigma_j \{ \psi^{\text{CDDB}}_{i,j} - \hat{\psi}^{\text{CDDB}}_j \},$$

where

$$\sigma_j = 0 \quad (j \leq 14, j \geq 30)$$

$$\sigma_j = \frac{j - 14}{6} \quad (15 \leq j \leq 19)$$

$$\sigma_j = \frac{j - 26}{4} \quad (27 \leq j \leq 29)$$

$$\sigma_j = 1 \quad (20 \leq j \leq 26).$$

Here, subscripts i and j refer to longitude and latitude points on the Gaussian grid, and the hat represents a zonal average at a given latitude. The forcing field was modified from the observed climate in this fashion to avoid some of the idiosyncrasies of forced barotropic models on the sphere. If the full observed zonal variation is retained in the Tropics, very large amplitude, westward propagating waves with zonal wavenumber confined to those just above the forced range, M in (2), can form in the Tropics and dominate the model behavior throughout much of the midlatitudes. The effects of retaining zonal variations in the polar regions are not so drastic, but some highly unrealistic (even by the standards of this model context) small-scale instabilities can result in the polar regions. Using the zonal forcing outside of the NH midlatitudes greatly reduces these problems without having significant impacts on the midlatitude behavior. A similar forcing could also be used to attempt a simulation of the Southern Hemisphere (SH) storm tracks; however, such results are not reported here.

The relation between the "zonalized" forcing fields and the corresponding observed monthly means is demonstrated in Fig. 1. Figure 1a depicts the observed January monthly mean 300-mb streamfunction, while Fig. 1b shows the corresponding forcing streamfunction for January, with regions outside the NH midlatitudes converted to the zonal mean.

c. *Normal-mode instability*

In the sections that follow, the linear normal modes (Simmons et al. 1983, hereafter SWB) of (2) are used in an attempt to explain the behavior of the model. The normal modes were computed for linearizations around the time-mean streamfunction $\bar{\psi}$ from extended integrations of (2). Computations were performed using an explicit matrix method for the T42 model. In a limited number of cases performed at T63 truncation, the iterative method of Anderson (1991) was used to find a set of the most unstable eigenmodes. Eigenvectors are displayed using the phase–magnitude plot format (SWB) in which contours represent the local amplitude of the eigenvector and vectors are used to represent the local relative phase.

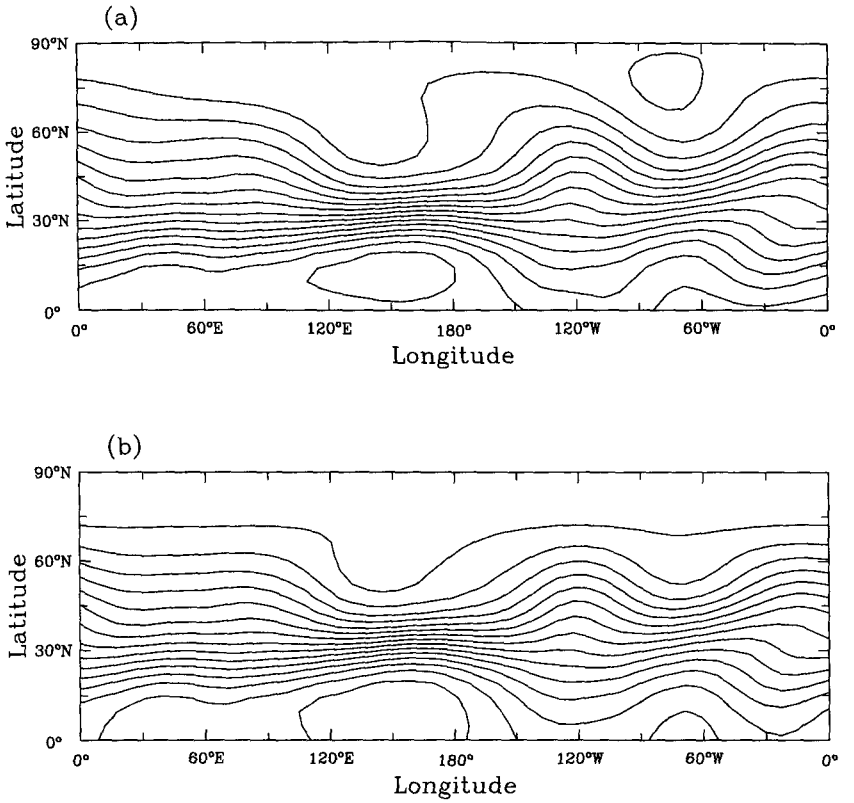

FIG. 1. (a) Observed 300-mb January CDDB climatological streamfunction ψ^{CDDB} and (b) the corresponding zonalized forcing field, ψ^F. The contour interval is 10^7 m^2 s^{-1}.

3. Control experiment

a. Model integrations

The forced, dissipative model [(2)] is integrated for the zonalized January monthly mean forcing, shown in Fig. 1b, with a T42 truncation. We refer to this model integration as the control run. The forcing strength α is 1×10^{-17} m^{-2} s^{-1}, and κ is chosen so that the smallest resolved wave is damped with an e-folding time of 1 day. The forcing is truncated at total wavenumber 10 and zonal wavenumber 4 [$N = 10, M = 4$ in (2)]. This value of M is chosen because a spectral analysis of the winter NH (Cai and Van den Dool 1992) shows that the spectral power of the stationary waves reduces sharply in the vicinity of zonal wavenumber 4 in the midlatitudes. The value of N was chosen so that the structure of the background flow maintained a fairly good representation of the structure of the stationary waves. Results in Anderson (1991) also suggest that this value is the most natural for defining the background flow in the context of barotropic normal-mode instability. The results presented are somewhat sensitive to the choice of M (see section 4) but show little sensitivity to the value of N. The model is integrated for 700 days, and data from the last 500 days are sampled at each model day; this integration is referred to as the control case.

The 500-day time-mean model streamfunction $\bar{\psi}$ (Fig. 2a) is very similar to the forcing (Fig. 1b) and observed (Fig. 1a) streamfunctions. The main difference is that the two oceanic jets are somewhat weaker in the time-mean flow of the barotropic model. Figure 2b shows the standard deviation of the transient streamfunction $\sigma(\psi')$, where the prime indicates deviation from $\bar{\psi}$. Despite the lack of baroclinic waves in this barotropic model, local maxima of $\sigma(\psi')$ are defined as the model's "storm track." There are three distinct latitudinal bands of locally enhanced σ: polar regions ($\phi > 75°$), midlatitudes ($30° < \phi < 60°$), and the subtropics ($\phi < 30°$).

The model's midlatitude storm tracks are certainly different from the observed storm tracks (see Fig. 6a), in particular over the Eurasian continent and the central Pacific. The local minimum of σ downstream of the Atlantic storm track, near 30°E, is not as pronounced as in the observations. The local maximum in the Pacific storm track appears about 60° upstream of its observed counterpart, although the latitude is similar to the observed. However, there are also a number of similarities between the model and observed storm tracks.

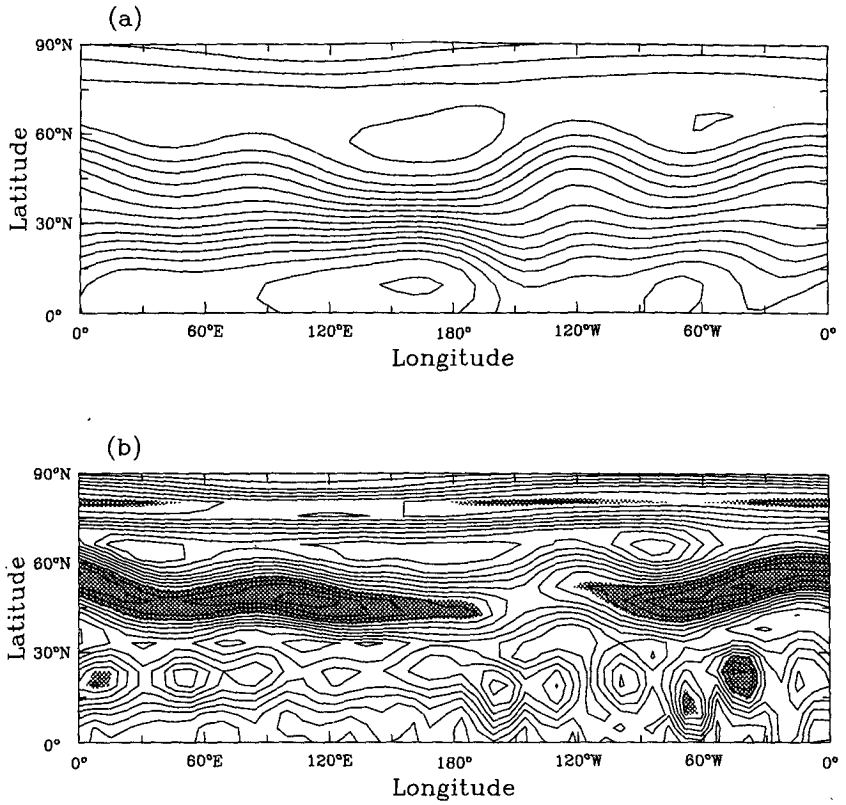

FIG. 2. (a) The 500-day time-mean streamfunction $\bar{\psi}$ and (b) standard deviation of the transient eddy streamfunction for the control case. The contour intervals are (a) 10^7 m^2 s^{-1} and (b) 1.5×10^5 m^2 s^{-1} with values greater than 1.6×10^6 m^2 s^{-1} shaded.

The structure and position of the Atlantic storm track and the local minimum between the Pacific and Atlantic storm tracks near 120°W are reproduced well by this model. In particular, the observed zonal orientation for the Pacific and SW–NE tilt for the Atlantic storm tracks are evident in the model.

An analysis of the midlatitude waves can help to explain the similarity between the storm tracks in this barotropic model and those in observations. Figure 3a shows the spectra of ψ' averaged over all frequency bands for a given zonal wavenumber at each latitude. There are three distinct regions of local maximum power: zonal wavenumber $k = 2$ in the polar region, $k = 5$ in the midlatitudes, and $k = 5$ and 6 in the subtropics. The spectra of ψ' averaged over all zonal wavenumbers for a given frequency at each latitude is shown in Fig. 3b. A distinct spectral peak is found once again in the polar and midlatitude regions, with periods of 3 and 4.8 days, respectively. In the subtropics there are three peaks that represent eastward propagating waves with periods of 4.8 and 20 days, and a westward propagating wave with period of 20 days. From Figs. 3a and 3b, it is clear that the midlatitude waves are dominated by zonal wavenumber 5 with a period of 4.8 days. There is also a small spectral peak at wavenumber 6 with a period of 3.3 days that is not visible in Fig. 3a. These zonal scales and periods are consistent with those of synoptic-scale waves in the atmosphere although the observed midlatitude transients do not exhibit the localized bull's-eye patterns seen in Fig. 3. As will be discussed in detail in section 4, this is at least partially due to the way in which this model is forced; waves that project on spherical harmonic components with wavenumbers smaller than M and N cannot evolve freely in this model.

b. Linear normal modes

The unstable normal modes of baroclinic models linearized around zonally varying basic states have been related to the observed storm tracks (Frederiksen 1983). Normal modes of the forced BVE linearized around zonally varying basics states have also been offered as a possible explanation for low-frequency variability in the atmosphere (SWB). SWB also described a weakly unstable barotropic mode that may be related to the storm tracks in the SH, however, they documented no unstable mode of synoptic spatial and temporal scales in the NH. The results of these earlier studies and the sharp spectral peak at $k = 5$ and $T = 4.8$

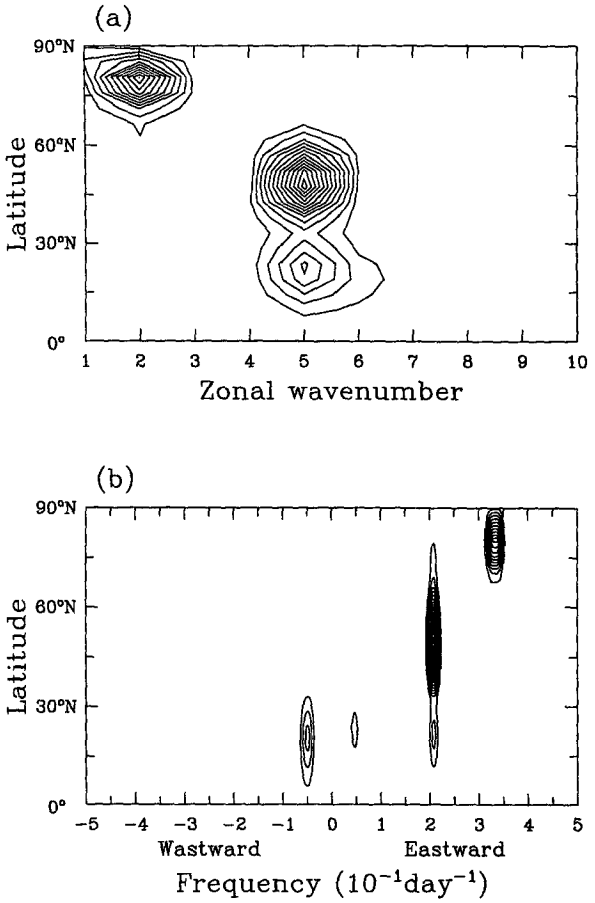

FIG. 3. Power spectrum of transient eddy streamfunction as a function of (a) latitude and zonal wavenumber and (b) latitude and frequency. The contour intervals are (a) 10^{11} m^4 s^{-2} and (b) 4×10^{11} m^4 s$^{-2} \cdot \Delta\omega^{-1}$.

days in midlatitudes (Fig. 3) motivate the examination of the normal-mode instability of the forced barotropic model. The normal modes described are for (2) linearized around the time-mean model streamfunction $\bar{\psi}$.

There are four unstable normal modes for the control case. The period, growth rate, dominant wavenumber, and description of these unstable modes are summarized in Table 1. The most unstable mode is found in the polar region and is consistent with the spectral analysis that shows a clear peak at zonal wavenumber 2 (Fig. 3a) and at a period of 3 days (Fig. 3b) north of 75°N. In addition, the structure of the transient eddy standard deviation in the polar region in Fig. 2b is similar to the amplitude of the most unstable linear mode (not shown). Therefore, it seems likely that the most unstable normal mode is directly responsible for the model behavior in the NH polar region.

There are also unstable modes in the NH subtropics. Comparison of the spectral analysis (Figs. 3a,b), and descriptions of the unstable modes in Table 1 suggest that the third and fourth unstable modes can at least partially explain the transient eddy structure in the subtropics (see Fig. 2b). However, there is no unstable normal mode that resembles the midlatitude storm track. In fact, none of the unstable modes has significant amplitude in the NH midlatitudes.

Although there is no unstable normal mode in the NH midlatitudes, large-amplitude neutral modes can be excited by various mechanisms and might offer an explanation for the model storm tracks. Figure 4 shows two decaying modes with e-folding decay times of 70 and 30 days, respectively. There are remarkable similarities between these two modes and the model's midlatitude storm track. In particular, the dominant zonal wavenumber and period of the slower decaying mode (Fig. 4b) are 5 and 4.8 days, which is quite close to those for the midlatitude spectral peaks shown in Figs. 3a,b. Therefore, it seems reasonable to conclude that these neutral modes are intimately related to the model's storm tracks. The two decaying modes in Fig. 4 are selected from a total set of over 1000, of which nearly 100 have similar decay rates. It would be interesting to understand why these two modes seem to play such a dominant role in the model's storm tracks.

Although the two modes just discussed are decaying, it might nevertheless be possible to explain their importance partially within the context of linear theory. Since the linear operator corresponding to (2) is not symmetric, the eigenvectors of the operator are not orthogonal. As noted in a number of previous works (Farrell 1984; Held 1985), the lack of orthogonality of modes can allow very large transient growth of even decaying modes in the linear model. As noted by Branstator (1985), the optimal perturbation for growth of a given normal mode is the corresponding mode from the adjoint of the linear operator. The adjoint eigenvectors corresponding to the storm track decaying modes have been computed. Both of the adjoint eigenvectors have significant amplitude only in the midlatitude regions where the forward problem eigenvectors have largest amplitude. Unfortunately, this linear result gives no ad-

TABLE 1. Period, e-folding times, dominant zonal wavenumbers, and a brief description of the four unstable linear normal modes for the control integration.

Period (days)	e-folding (days)	Dominant wavenumber	Description
3.1	11.4	2	NH polar, eastward propagating
12.3	208.5	5 or 6	Two bands about 20°N and 30°S; appears to originate in Tropics
19.0	48.8	About 5	Band at 40°S, isolated centers at 20°N
22.3	402	About 6; 1	NH polar eastward wave 1; isolated wave 6 at 20°N

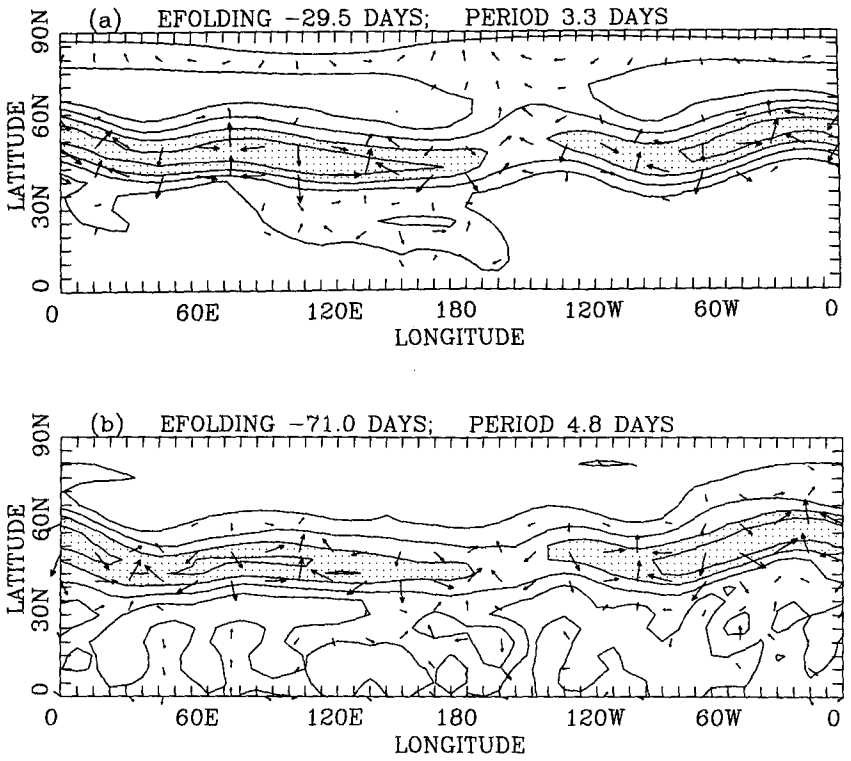

FIG. 4. Phase–magnitude plots for two decaying modes of the T42 barotropic model. Contours are local magnitude of the eigenvector with interval one-fifth of the maximum magnitude. Regions with amplitude greater than 0.6 times the maximum are stippled. Arrows give local phase of eigenvector.

ditional insight into the mechanism by which these two normal modes might be excited, although they need not necessarily be optimally excited to gain a large amplitude (Held 1985).

It is probable, therefore, that the storm track decaying modes are excited by some nonlinear mechanism. The primary energy source in the forced barotropic model is the production of eddy energy from the mean flow via the unstable linear modes in the NH polar regions and in the subtropics. Some sort of nonlinear resonance between the decaying storm track modes and waves propagating out of the unstable regions can result in the concentration of energy in the storm track modes. Rather than pursue this possibility in the context of the normal modes, an explicit examination of the dynamics of wave propagation is presented in the next section.

c. *Barotropic Rossby waveguides*

The normal-mode analysis of the previous section can be complemented by examining the relation of the model's transient eddies to the background flow. In light of the results of observational and modeling studies (Dole 1986; Lau 1988; Lee 1995; Branstator 1995), it is relevant to examine the model's time-mean flow for the presence of a barotropic Rossby "waveguide" with wave propagation characteristics corresponding to the structure of the model's storm tracks. The refractive index must be explicitly calculated in order to see if the barotropic Rossby waveguide can explain the storm track structure. It is necessary to assume that the background flow varies slowly both in longitude and latitude compared with the scale of the waves propagating through the inhomogeneous medium as in Karoly (1983) and Branstator (1983). Furthermore, assuming that the ratios of meridional to zonal wind and zonal to meridional vorticity gradient are small, the perturbation vorticity equation linearized about the time-mean flow is

$$\frac{\partial \nabla^2 \psi'}{\partial t} + \bar{u}\frac{\partial \nabla^2 \psi'}{\partial \lambda} + \frac{1}{a^2 \cos\varphi}\frac{\partial \psi'}{\partial \lambda}\frac{\partial \bar{q}}{\partial \varphi} \approx 0, \quad (3)$$

ignoring the diffusion and the thermal damping. Here λ and φ are the longitude and latitude, a is the earth's radius, q is the absolute vorticity, and the overbar and prime represent the time mean and departures from that mean. Assuming a plane wave solution in the longitudinal direction,

$$\psi' = \Psi(\varphi)e^{i(m\lambda - \omega t)},$$

and using (3) gives

$$\frac{d^2\Psi}{ds^2} + n^2 = 0,$$

where the refractive index for meridional propagation is

$$n^2 = \left(\frac{\cos\varphi}{\bar{u} - c}\right)\frac{\partial \bar{q}}{\partial \varphi} - m^2 \qquad (4)$$

and

$$s = \ln\left(\frac{1 + \sin\varphi}{\cos\varphi}\right).$$

Here c is the phase velocity defined as ω/m. Essentially the same equation was derived to study propagation of low-frequency disturbances in a slowly varying background flow (Branstator 1983; Hoskins and Ambrizzi 1993) except that c was set equal to zero in these studies. Before we present the calculations, it should be noted that the transient eddies do not have to fill the entire propagation region indicated by the refractive index; the refractive index simply tells us that disturbances with certain values of zonal and meridional wavenumbers can propagate in some selected regions.

Figure 5a shows the refractive index, $\mathrm{sgn}(n^2)|n|$, for $\omega = 2\pi/4.8$ days^{-1} and $m = 5$ (see Fig. 3). The contours are plotted only in the propagating region, that is, where $n^2 > 0$. Also, regions where $0 \leq n \leq 6$ are shaded to distinguish the region where n^2 is relatively small. In the same figure, the thick solid line that results from the concentration of many contours indicates the location of the critical latitudes. The basic-state meridional potential vorticity gradient $\partial\bar{q}/\partial y$ is shown in Fig. 5b. The region of positive n^2 lies over the positive $\partial\bar{q}/\partial y$ region in most of the NH except for the small area north of 60°N. The zonal band of negative $\partial\bar{q}/\partial y$ between 60° and 70°N is unrealistic (cf. with Fig. 6c for the observed flow, $\partial q^{\mathrm{CDDB}}/\partial y$; the meridional potential vorticity gradient for the zonalized climatological basic state is very similar to Fig. 6c). Nevertheless, the refractive index shows many key similarities between the barotropic model and the observations.

Comparing Fig. 5a with Fig. 2b, there is a reasonable similarity between the model's storm track and the propagating region. For better comparison, these two fields are plotted in Fig. 5c where the model's storm track is indicated by gray-scale shading. In these figures, poleward excursions of the storm track at $\lambda = 0°$, 90°E, and 120°W, and equatorward excursions of the storm track at $\lambda = 40°$E and 70°W are clear in both fields. This result suggests that the barotropic waveguide may be responsible for the model's storm tracks.

To examine whether propagation of transient eddies through the waveguide plays an important role in determining the storm track structure, we diagnose the wave activity as formulated by Plumb (1986), applied to a barotropic flow

$$\frac{\partial \mathcal{A}}{\partial t} + \nabla\cdot\mathbf{M}_T = S_M,$$

where $\mathcal{A} = \cos\varphi\ [(\overline{\zeta'^2}/2)/|\nabla_H\bar{q}|]$, S_M represents wave activity sources and sinks,

$$M_T = M_R + \bar{u}\mathcal{A},$$

$$M_R = \cos\varphi\left(n_1\overline{u'v'} + n_2\frac{\overline{v'^2 - u'^2}}{2}, \; n_1\frac{\overline{v'^2 - u'^2}}{2} - n_2\overline{u'v'}\right),$$

with

$$n_1 = \frac{\partial\bar{q}/\partial x}{|\nabla_H\bar{q}|} \quad \text{and} \quad n_2 = \frac{\partial\bar{q}/\partial y}{|\nabla_H\bar{q}|}.$$

Figure 7a shows the wave activity $\mathcal{A}$ and the total wave activity flux vector M_T, which is everywhere parallel to group velocity in the Wentzel–Kramers–Brillouin (WKB) limit. The structure of M is somewhat different from that of the transient streamfunction variance. In particular, the center of the Pacific storm track as specified by $\mathcal{A}$ is at 150°E rather than 120°E. However, the main features of the storm track remain intact. The M_T vectors point downstream everywhere, closely following the midlatitude storm track, and their magnitude is greater than those of M_R (see Fig. 7b) by at least an order of magnitude. Furthermore, away from the regions of the local maxima of $\mathcal{A}$, the magnitudes of the M_T vectors remain large, indicating that the structure of the midlatitude storm track in this model is by and large determined by advection of wave activity by the time-mean flow.

Given the success of the barotropic waveguide as an explanation for the model storm tracks, the relevance of the barotropic waveguide in the atmosphere is examined. The refractive index computed using the observed January climatology is shown in Fig. 6b, once again for $\omega = 2\pi/4.8$ days^{-1} and $m = 5$ for comparison with Fig. 5a. The horizontal structure of the waveguide for this observed climatological basic state is very similar to that for the time-mean basic state of the barotropic model (cf. Fig. 6b with Fig. 5a). The main similarities are the poleward excursion of the waveguide at 120°W and between $\lambda = 0°$ and 90°E and the critical latitudes on the equatorward side of the jet between the date line and 60°W. Primary differences are that in the barotropic model the poleward extension of the waveguide is displaced a few degrees to the north, a narrow evanescent region exists in midlatitudes between $150°\mathrm{W} < \lambda < 30°\mathrm{W}$, and the critical latitude between $30°\mathrm{W} < \lambda < 60°$E along 45°N is absent. Comparing the observed and the model, it seems plausible that barotropic dynamics can play a crucial role in determining the structure of the observed midlatitude storm tracks in the Western Hemisphere. As mentioned ear-

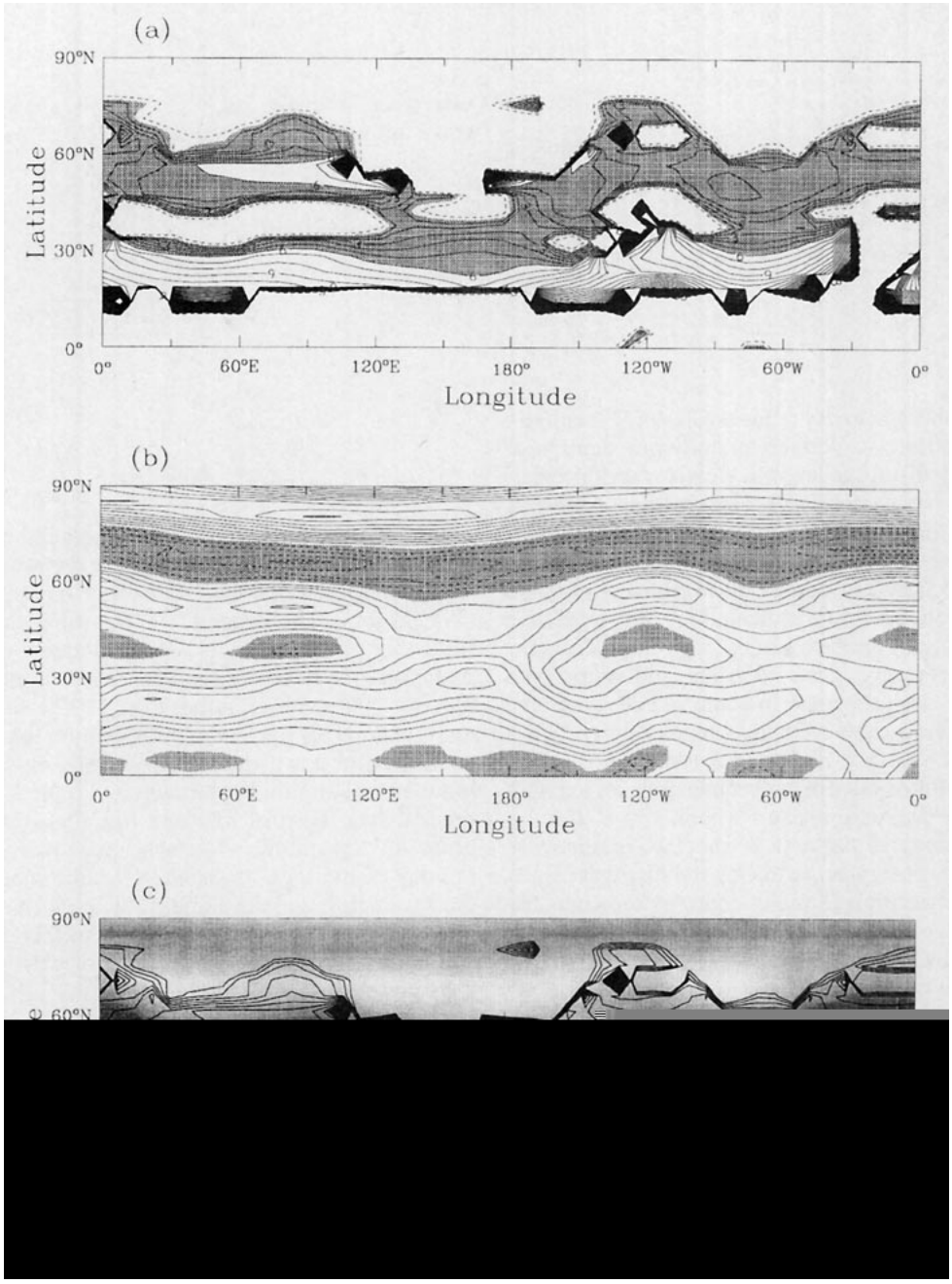

FIG. 5. (a) Refractive index, $\text{sign}(n^2)|n|$ for $k = 5$ and $T = 4.8$ days, (b) meridional potential vorticity gradient, and (c) superposition of (a) and the standard deviation of the transient eddy streamfunction (shown in Fig. 2b), for the time-mean flow of the control case. The contour intervals are (a) 1, (b) 10^{-11} m^{-1} s^{-1}, and (c) 1. In (a), values less than -1 are not contoured, and values greater than 0 but less than 6 are shaded. In (b), negative values are shaded. In (c), gray-scale shading is used for the standard deviation of the transient eddy streamfunction.

lier, the Pacific storm track in the model is located too far upstream compared with that in the atmosphere. Consistent with this, in the midlatitude central Pacific where the observed Pacific storm track is located, the model refractive index is negative, indicating wave evanescence (cf. Figs. 5a and 6b). This implies that barotropic dynamics may be less relevant to the Pacific storm track than to the Atlantic storm track.

Not only the structure of the model's storm track, but also the structure of the individual eddies in the model is consistent with the barotropic waveguide. Figure 8 shows one-point correlation maps of the eddy

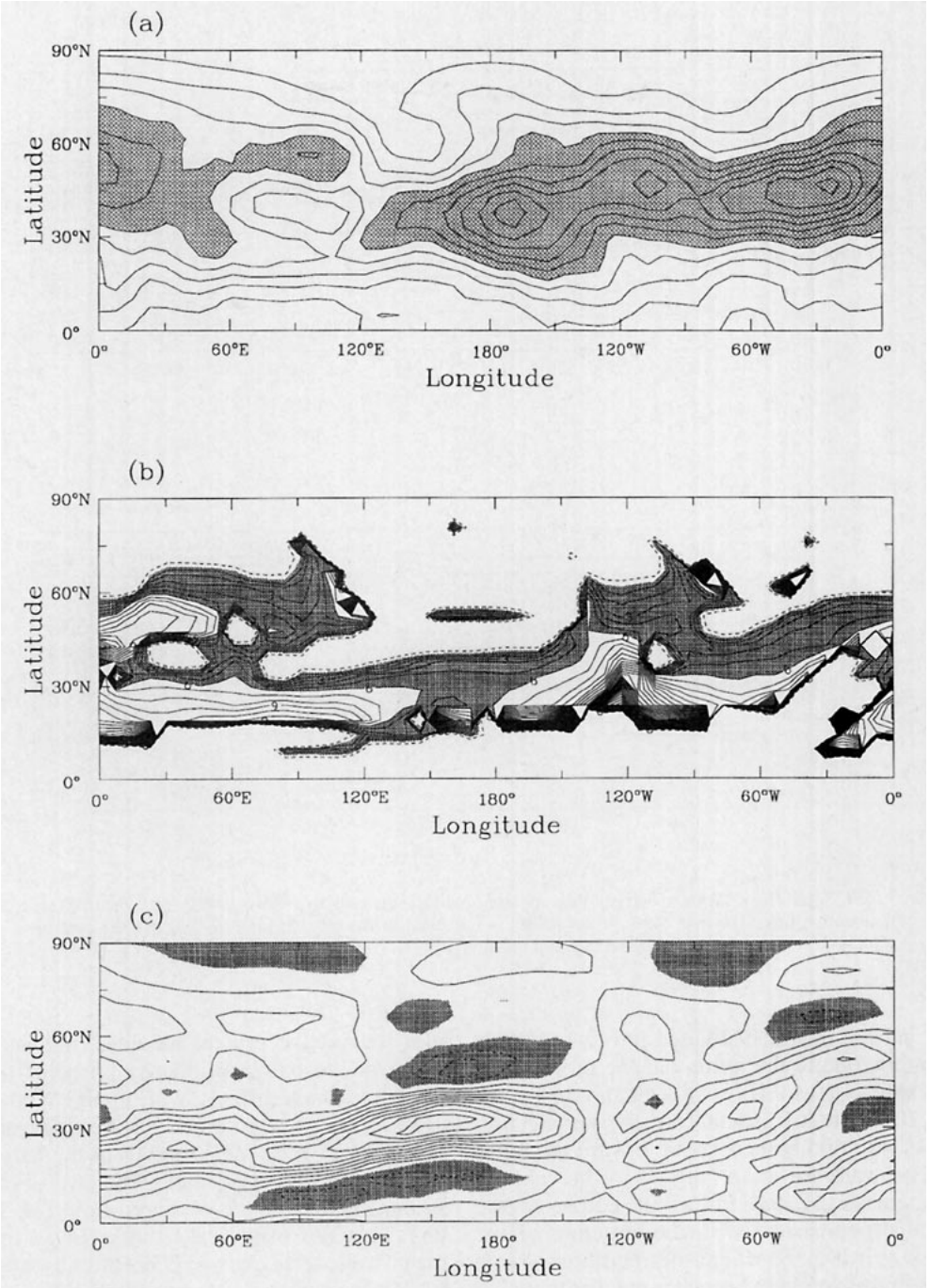

FIG. 6. (a) Standard deviation of the 2–6-day bandpass eddy streamfunction for the 300-mb January flow averaged from 1985 to 1992. (b) Refractive index, $\text{sign}(n^2)|n|$ for $k = 5$ and $T = 4.8$ days, and (c) meridional potential vorticity gradient for the observed January flow ψ^{CDDB}. The contour intervals are (a) 4×10^5 m^2 s^{-1}, (b) 1, and (c) 10^{-11} m^{-1} s^{-1}. In (a), values greater than 2.8×10^6 m^2 s^{-1} are shaded. In (b), values less than -1 are not contoured, and values greater than 0 but less than 6 are shaded. In (c), negative values are shaded.

(deviation from the time mean) vorticity field with the base point at 45°N, 90°W. The qualitative structure of the vorticity field shown in Fig. 8 is insensitive to the choice of the longitudinal position of the base point.

In the model's Pacific storm track, the vorticity starts to be stretched NE–SW between 150°E and 180°; the positive vorticity centered at 160°E at lag -2 day (Fig. 8) is stretched near 180° at lag 0 as it propagates toward

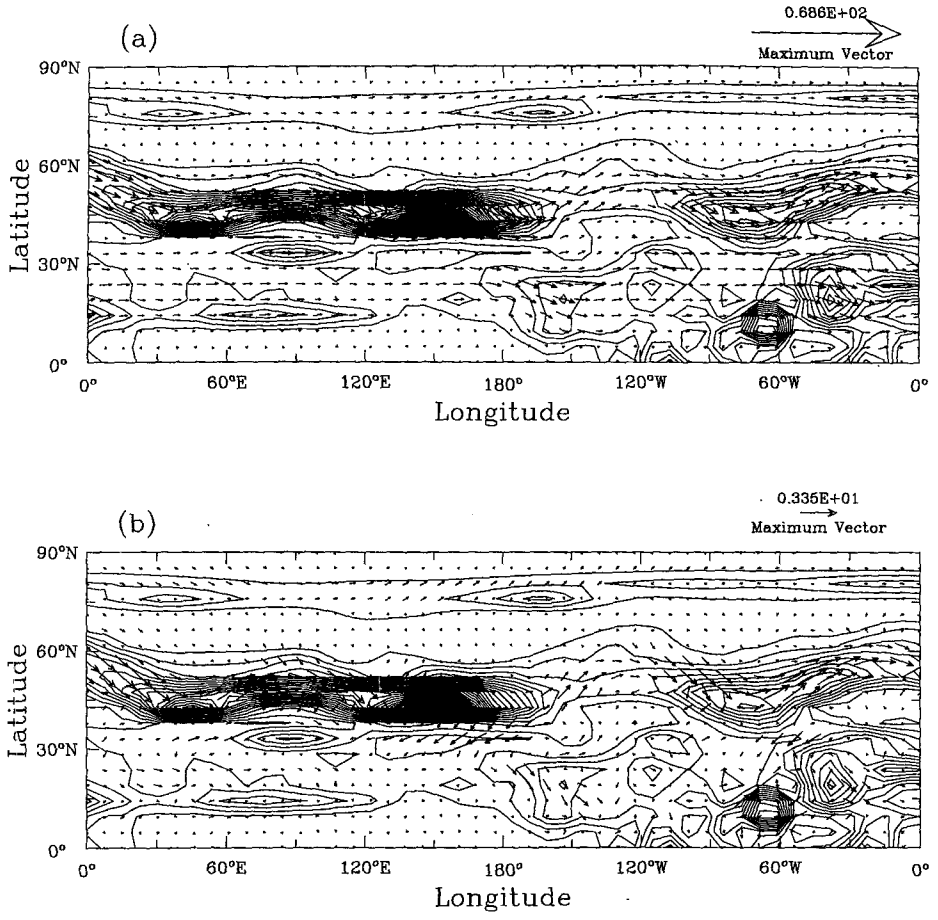

FIG. 7. (a) The total wave activity flux vector M_T and (b) the radiative wave activity flux vector M_R for the control case. The maximum vector length is indicated in the plot. In both (a) and (b), the contours represent the wave activity M, and the contour interval is 6×10^{-2} m s^{-1}.

the east. At lag +2 day, it is divided into two distinct vorticity centers, one to the north and the other to the south. This split is reasonably well diagnosed by the waveguide. Between 150°E and 180° the propagating region is split into two branches, one toward the north and the other toward the south (Fig. 5a). The value of n becomes increasingly large toward the equator in the southern branch, consistent with the structure of the vorticity shown in Fig. 8, where the meridional scale of the eddies in this southern branch is smaller than that in the northern branch. As the disturbances encounter the critical latitudes in the subtropics, they tend to be dissipated.

These results strongly suggest that the meridional eddy stretching due to the two-way split of the waveguide plays an important role in forming the local minimum of storm track amplitude near 150°W, consistent with the idealized model study of Lee (1995). It is of particular interest to note that the equatorward barotropic decay in the eastern Pacific can occur due to the waveguide effect of the background flow pushing eddies toward the critical latitudes, not necessarily because of the barotropic decay phase of the nonlinear baroclinic wave life cycle (Lim and Wallace 1991).

In contrast to the central Pacific, there are no critical latitudes between 30°W and 0° in the barotropic model's time-mean basic state, while critical latitudes exist in that region for the observed flow (cf. Figs. 5a and 6b). This lack of critical latitudes in the model's time-mean basic state may explain the absence of a storm track minimum downstream of the Atlantic storm track, especially since critical latitudes in the observations are near 45°N (see Fig. 6b), close to the latitude of Atlantic storm track termination.

Undoubtedly, not all aspects of the structure of the model's midlatitude eddies are realistic. In particular, in the Atlantic storm track region, the structure of the eddies is NE–SW (NW–SE) on the poleward (equatorward) side of the northern branch of the jet, so that eddies are extracting energy barotropically from the basic flow; the opposite is true in observations. However, this barotropic model does tell us that locally excited

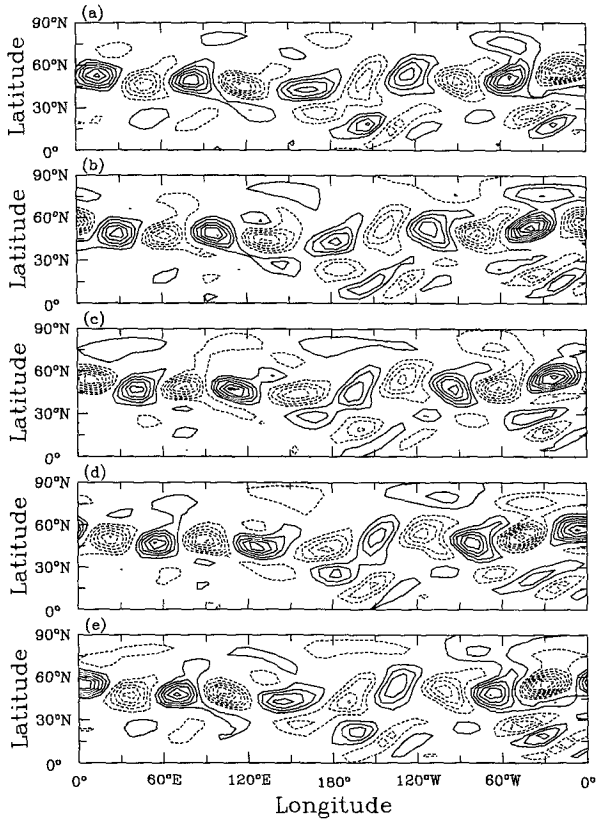

FIG. 8. Time-lagged, one-point covariance map of the transient eddy relative vorticity for the control case at (a) −2, (b) −1, (c) 0, (d) 1, and (e) 2 days. The base point is at 90°W and 45°N. The contour interval is 3×10^{-12} s^{-2}.

baroclinically unstable eddies in the two oceanic storm track regions (Frederiksen 1983) may not be essential ingredients for the formation of the storm tracks. Regardless of the locations and causes of synoptic-scale eddy generation, the waveguide can lead to the formation of moderately realistic midlatitude storm tracks.

4. Sensitivity tests

a. Sensitivity to the model parameters

The sensitivity of the results above to changes in a number of parameters of the barotropic model is examined in this section. Parameters examined include diffusion, forcing strength, forcing truncation, and truncation of the model.

In addition to the control integration that had a diffusion that damped the smallest resolved T42 wave with a 1-day e-folding time, additional cases with damping times of 0.5, 2, 5, and 10 days are examined. All additional runs are qualitatively similar to the control run in terms of the standard deviation of the eddy streamfunction; in particular, all four display the distinct minimum over the eastern Pacific. The details of the linear normal modes were much more sensitive to the changes in diffusion than were the model storm tracks. For example, in the 5-day damping case, there is a weakly unstable mode with an e-folding time of 99 days and a period of 3.4 days that shows similar structure to that of the storm tracks. The structure of the unstable mode is very similar to that shown in Fig. 4b. Although the details of the linear normal modes have changed, the conclusions of section 3b seem to extend gracefully to this case; this is consistent with the remaining diffusion cases that are not discussed in detail here.

Spectral analysis of the midlatitude transients in the 5-day damping case (not shown) indicates that there are spectral peaks at $k = 6$, $T = 3.4$ day, as well as at $k = 5$, $T = 4.8$ day in the midlatitudes. The combination of these two waves gives rise to wave packets, instead of the essentially uniform wave train in the control case. Figure 9 shows the one-point correlation maps, once again with the base point at 90°W and 45°N. Although the eddies now form a wave packet as in Lee and Held (1993), one still sees the north–south split of the eddies in the eastern Pacific. The refractive index (not shown) for both $k = 5$, $T = 4.8$ day and $k = 6$, $T = 3.4$ day remains qualitatively similar to that shown

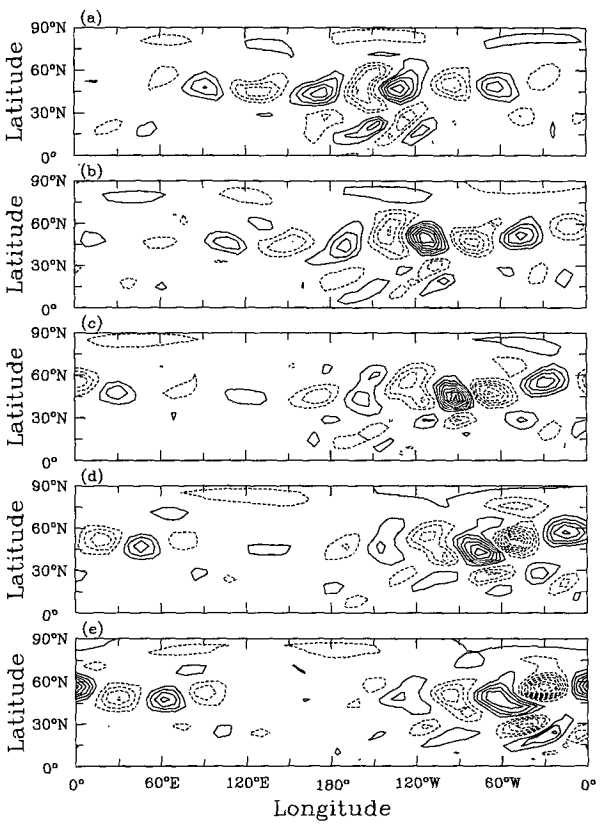

FIG. 9. As in Fig. 8 but for the case with a 5-day diffusive damping.

in Fig. 5a. Although the details of the eddies have changed, the relation between the refractive index and the storm tracks is essentially unchanged from the control; similar results were found for the other varied diffusion cases.

The sensitivity of the results to changes in the forcing strength is examined with two additional integrations: one case with reduced forcing, $\alpha = 5 \times 10^{-18}$, and another with increased forcing, $\alpha = 1.2 \times 10^{-17}$. As in the varied diffusion cases, the structure of the midlatitude storm tracks was found to be qualitatively similar to that for the control case for both stronger and weaker forcing. For both cases, the midlatitude disturbances are strongest at $k = 5$, $T = 4.8$ days, and the basic structure of the time-mean flow refractive index remains unchanged. As for the diffusion results, the sensitivity of the linear normal modes is considerably greater. For the weaker forcing, there is a weakly unstable mode that is similar to the one in the reduced diffusion case. In the stronger forcing case, there does not seem to be a single normal mode that is similar in period and structure to those discussed above. Again, this demonstrates that the basic storm track structure is robust, even though the normal modes that appear to be responsible may be quite sensitive to model details.

An additional parameter in this model is the truncation of the forcing. Some justification for truncating the forcing in the control case at $N = 10$ and $M = 4$ was presented in section 3. However, because the dominant transient midlatitude wave's zonal wavenumber is 5 (the smallest zonal wavenumber that is entirely free in the forced model), it is particularly interesting to find out how sensitive this wave is to the value of M. Therefore, N is fixed at 10 while the value of M is varied. For the case of $M = 3$, the dominant zonal wavenumber in midlatitudes is 4, instead of 5 (Fig. 10a), with a period of 8.3 days, clearly indicating that the dominant zonal wavenumber in this model is sensitive to the choice of M. However, the qualitative structure of the midlatitude storm tracks in this model resembles that of the control case, and the waveguide (not shown) for $k = 4$, $T = 8.3$ days is quite similar to that for $k = 5$, $T = 4.8$ day of the control experiment (Fig. 5a). When M is further reduced to 2, the zonal variation in the time-mean state was very small. This is hardly surprising since the forcing, which is the model's only information about zonal variations, contains only two zonal waves. For the $M = 2$ case, significant changes in storm track structure occur, for instance, the local minimum lies in the western Pacific instead of the eastern Pacific (Fig. 11). However, the dominant zonal wavenumber is still 4 instead of 3 (Fig. 10b). This suggests that the upscale energy cascade halts near $k = 4$. It is interesting to observe in this model that $k = 4$ corresponds both to the scale of the stationary wave and to the scale at which the upscale energy cascade is halted.

The final set of sensitivity experiments examines the effects of the model's truncation. The control case and

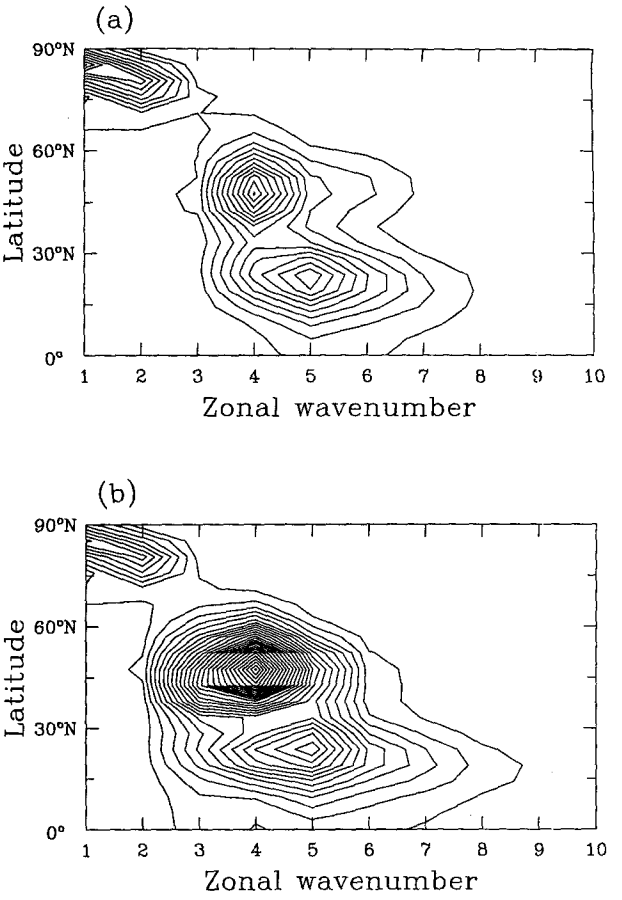

FIG. 10. Power spectrum of transient eddy streamfunction as a function of latitude and zonal wavenumber for (a) the $M = 3$ case and (b) the $M = 2$ case. The contour interval is 10^{11} m^4 s^{-2}.

all of the sensitivity runs described above have been integrated in T21 and T63 versions of the model in addition to the T42 cases discussed previously. In all cases, the forcing is truncated at T21. The T21 results display similar storm tracks to the T42 in most cases (although a few were drastically different from the T42), and the T21 cases had many more unstable normal modes, consistent with the findings of Anderson (1991). The T63 results are all extremely similar to their T42 counterparts, suggesting that T42 is sufficiently high resolution for these integrations. Because of expense, only a subset of the most unstable modes of the T63 integrations have been computed. The T63 modes are very similar to the T42 most unstable modes, again consistent with Anderson (1991).

b. Sensitivity to the basic-state forcing

This section describes the behavior of the control model's storm tracks for different winter forcing fields, namely the "zonalized" CDDB climatologies for November, December, February, and March. The NH

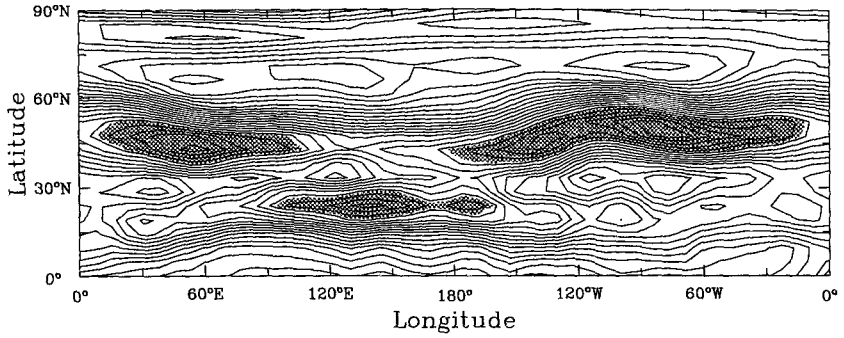

FIG. 11. Standard deviation of the transient streamfunction for the $M = 2$ case. The contour interval is 1.5×10^5 m^2 s^{-1}. Shading denotes values greater than 3.2×10^6 m^2 s^{-1}.

midlatitude storm tracks from the model integrations forced by the December, February, and March climatologies are very similar to those for the January climatology (Fig. 2b). For these other winter months, the dominant zonal wavenumber of the midlatitude transients is again 5. The corresponding periods are 4.8, 5.7, and 5.5 days for December, February, and March, respectively. The structure of the waveguides for the time-mean states of the model for these three months are also similar to that for the January case (Fig. 5a).

A distinctly different situation is found for the November climatology; a midlatitude storm track barely exists (Fig. 12). Not only is the amplitude of the streamfunction standard deviation much smaller than for the other months, but also the structure is vastly different. Spectral analysis indicates that in the midlatitudes the dominant zonal wavenumber is still 5, but the wave periods range between -6 and 3.3 days (not shown); the negative period indicates westward propagating waves. The refractive index for $m = 5$, $T = 4.3$ (spectral power is highest at a period of 4.3 days) is shown in Fig. 13a. The structure of the midlatitude waveguide in this case is certainly different from that of the January case (Fig. 5a) and does not resemble the observed storm track. However, the waveguide is not inconsistent with the model's storm track for the November case (Fig. 12).

As described in Nakamura (1992), the two oceanic storm tracks are stronger in November than during midwinter, while their structure is similar to that in other winter months, except that the November storm tracks are displaced somewhat poleward. The November case indicates that, although the barotropic waveguide is related to the model's storm track, the barotropic model used in this study is not always capable of capturing important features of the observed storm tracks. There are several possible interpretations for this behavior. First, baroclinicity may be essential to the formation of storm tracks during November but not during the other winter months. Second, the barotropically unstable waves in the model forced by the November climatology might have modified the forcing flow so much that the time-mean flow no longer retains the barotropic waveguide that is required for the midlatitude storm track. Figure 14 shows $\bar{\psi}$ and ψ^F for November. As for the January case, weakened horizontal gradients of $\bar{\psi}$ compared with that of ψ^F indicate that barotropic transient eddies in the model tend to smooth the forced flow. For the November case, however, the reduction of horizontal gradients from ψ^F to $\bar{\psi}$ is much greater

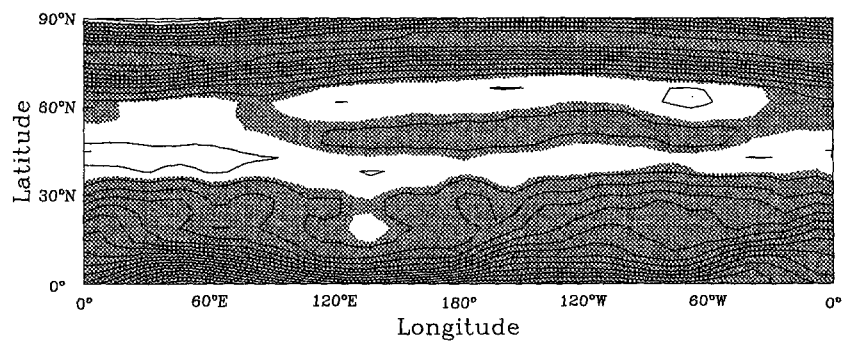

FIG. 12. Standard deviation of the transient streamfunction for the November case. The contour interval is 1.5×10^5 m^2 s^{-1}. Shading denotes values greater than 0.4×10^6 m^2 s^{-1}.

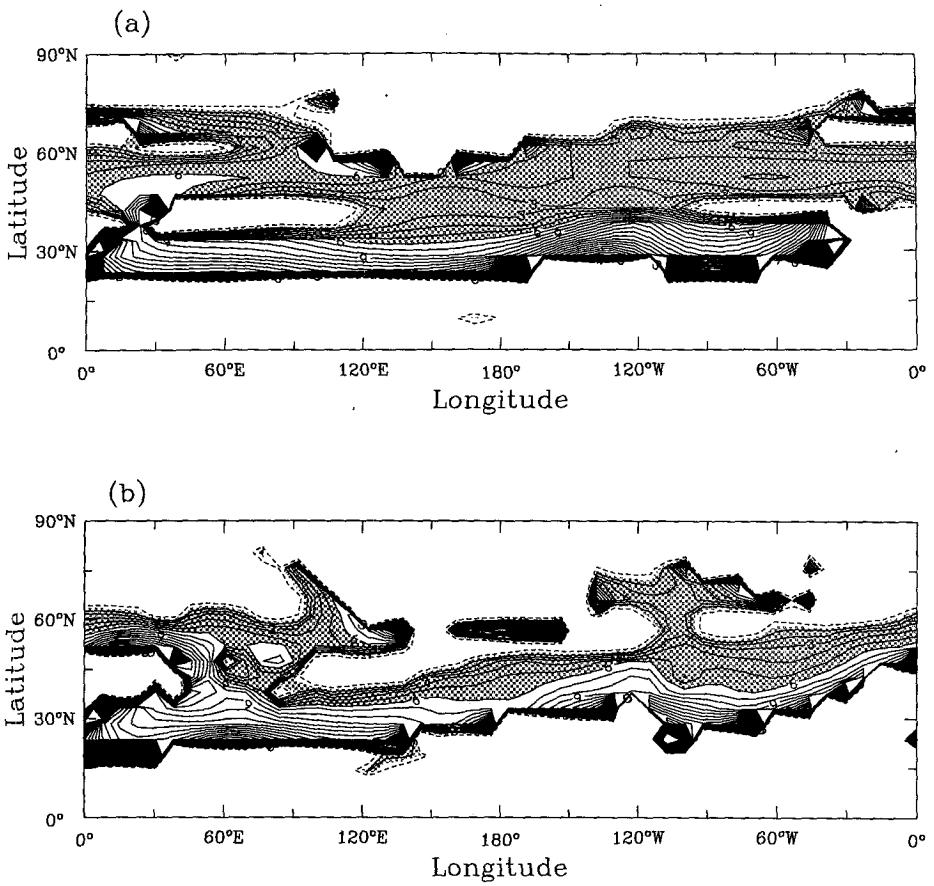

FIG. 13. Refractive index, $\mathrm{sgn}(n^2)|n|$, for $k = 5$ and $T = 4.3$ day for (a) the model time mean and (b) the observed flows for the November case. Contours and shading as in Fig. 5a.

than is the case for the other four months examined. The resulting November $\bar{\psi}$ is quite possibly too weak to steer the barotropic eddies into a recognizable storm track. Using an idealized model, Lee (1995) shows that the formation of localized storm tracks can be very sensitive to the strength of the deformation of the background flow. Therefore, it is possible that the structure of the observed storm track could be reasonably well simulated even for the November climatological flow if $\bar{\psi}$ in this model were closer to the observed climatology ψ^{CDDB}. The refractive index for $m = 5$, $T = 4.3$ for the November ψ^{CDDB}, shown in Fig. 13b, appears to support this conjecture, as there are stronger zonal variations of the waveguide including SW–NE tilting in the Atlantic storm track region.

Additional problems with the November storm track simulation may occur because the linear normal modes of the relatively smooth November time mean are much less unstable than is the case for January. This lack of instability may reduce the amplitude of the barotropic eddies, resulting in weak storm tracks even in those regions where the eddies can propagate.

5. Concluding remarks

In this study, a barotropic model forced with a modified 300-mb January climatology is able to simulate the NH midlatitude storm track structure reasonably well. These results demonstrate that the locally enhanced baroclinic regions that usually appear upstream of the observed storm tracks may not be essential for determining the structure of the storm tracks.

The linear normal modes of the barotropic model linearized around its time mean were computed to gain additional insight into the mechanisms forming the storm tracks. Unstable normal modes were found in the NH polar regions and in the subtropics, but there are no unstable modes with significant amplitude in the storm track regions. However, a pair of decaying normal modes exists that is extremely similar to the observed storm tracks. Apparently, these decaying modes are excited through nonlinear interactions with the unstable normal modes outside of the midlatitudes. Clearly, the barotropically unstable modes in the polar and subtropical regions are unrealistic, and there is little

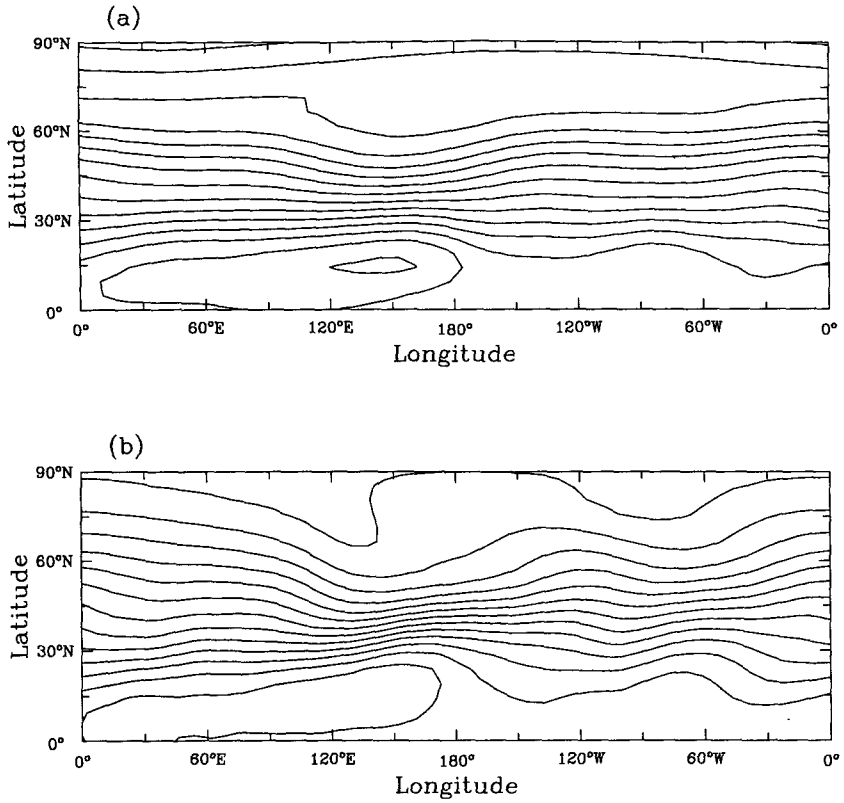

FIG. 14. (a) Model time mean and (b) observed 300-mb streamfunction for November. The contour interval is 10^7 m^2 s^{-1}.

doubt that the precise mechanism by which the midlatitude storm tracks emerge in this model is irrelevant for the atmosphere. However, the results demonstrate that barotropic effects can act to organize storm tracks through the impact of the time-mean flow on transient eddies, regardless of the precise location and mechanisms of eddy generation.

In the present study, a forced nonlinear model was used to demonstrate the possibility of storm track generation through barotropic waveguide effects. In a recent study, Branstator (1995) examined formation of storm tracks using a linear initial value problem. Applying the method described by Branstator (1995) to the forced barotropic model described in this paper results in areas of enhanced transient eddy variance that are qualitatively consistent with the results of the nonlinear integrations described here (Y.-Q. Zhang and I. M. Held 1995, personal communication). While the linear initial value problem described in Branstator can clearly elucidate the steering effect on storm track eddies, the linear initial value approach is not guaranteed to reproduce the nonlinear behavior of the system. In particular, the method of Branstator requires the specification of an arbitrary integration time to obtain a reasonable storm track structure in the linear model. Therefore, the results of fully nonlinear integrations such as the ones described here are of paramount interest, although the results of the forced nonlinear model are less straightforward to interpret than those of the linear initial value problem.

A barotropic waveguide, defined by the refractive index under the WKB assumption, resembles the structure of the model storm tracks. Somewhat similar results are found by applying the same method to observations. This suggests that the midlatitude storm tracks are rather tightly controlled by the barotropic waveguide, and once a disturbance is excited or introduced in this waveguide, at least in the Western Hemisphere, it propagates and disperses in a fashion consistent with the storm tracks. Even if a midlatitude disturbance is excited away from the enhanced baroclinicity region that is associated with the observed storm tracks, it may be constrained to evolve following the barotropic waveguide.

A closer examination of the model's storm track at once reveals that its "Pacific storm track" peaks 60° upstream of the observed, and the local minimum downstream of the "Atlantic storm track" is not sufficiently pronounced. It seems reasonable to assume that these differences can be explained by local baroclinic instability (e.g., Pierrehumbert 1984; Cai and Mak 1990) and/or baroclinic modulation, such as

"type B" cyclogenesis. Also, the barotropic model employed here cannot always capture the structure of the observed midlatitude storm tracks; sensitivity tests indicate that a model forced by a modified November climatology fails to mimic the observed storm tracks. There are at least two possible explanations for this behavior. First, baroclinicity may be more important for the formation of storm tracks during November than during any other winter months. Second, the barotropically unstable waves in the model forced by the November climatology have modified the forcing climatological flow strongly enough that the modified flow no longer retains an appropriate barotropic waveguide, which is required for the midlatitude storm track.

The barotropic model does not exhibit any dramatic sensitivity to the strength of the diffusion and forcing. Truncation of the forcing is more problematic since waves longer than the forcing truncation do not evolve freely. As a result, if the scale of the forcing truncation is smaller than the scale at which the upscale energy cascade should halt, the dominant scale of the transient waves may be artificially determined by the truncation. In the NH winter, the spectral power of the stationary waves declines sharply near zonal wavenumber 4 and the zonal wavenumbers of the dominant synoptic-scale waves are between 5 and 7. In the barotropic model used here, the forcing truncation for the zonal wavenumber is 4, and it follows that the dominant zonal wavenumber in the model is 5, close to the observed synoptic-scale waves.

Because the barotropic model used in this study is nonlinear and also possesses barotropic instability, it is difficult to separate the simple advection effect noted in Lee (1995) from other mechanisms of storm track formation involving unstable linear modes. However, given the relevance of barotropic dynamics for the observed storm tracks, as suggested in this study and in other recent papers (Lee 1995; Whitaker and Dole 1995; Branstator 1995), further modeling efforts should be undertaken in order to understand better the barotropic impacts on observed storm track dynamics. An interesting companion to the present study would make use of a similar forced barotropic model in which the dissipation was large enough to eliminate any instability. An additional "external" source of eddies could then be added to the model. In this more controlled experiment, better insight into the storm track formation problem may be obtained.

Acknowledgments. The comments by three anonymous reviewers improved this manuscript. S. Lee was partially supported by the National Science Foundation through Grant ATM-9525977.

REFERENCES

Anderson, J. L., 1991: The robustness of barotropic modes in a zonally varying atmosphere. *J. Atmos. Sci.*, **48,** 2393–2410.

——, 1995: A simulation of atmospheric blocking with a forced barotropic model. *J. Atmos. Sci.*, **52,** 2593–2608.

Branstator, G., 1983: Horizontal energy propagation in a barotropic atmosphere with meridional and zonal structure. *J. Atmos. Sci.*, **40,** 1689–1708.

——, 1985: Analysis of general circulation model sea surface temperature anomaly simulations using a linear model. Part II: Eigenanalysis. *J. Atmos. Sci.*, **42,** 2242–2254.

——, 1995: Organization of storm track anomalies by recurring low-frequency circulation anomalies. *J. Atmos. Sci.*, **52,** 207–226.

Cai, M., and M. Mak, 1990: On the basic dynamics of regional cyclogenesis. *J. Atmos. Sci.*, **47,** 1417–1442.

——, and M. H. Van den Dool, 1992: Low-frequency waves and traveling storm tracks. Part II: Three-dimensional structure. *J. Atmos. Sci.*, **49,** 2506–2524.

Chelliah, M., 1990: Seasonal climate summary: The global climate for June–August 1989: A season of near normal conditions in the tropical Pacific. *J. Climate,* **3,** 138–162.

Dole, R. M., 1986: Persistent anomalies of the extratropical Northern Hemisphere wintertime circulation: Structure. *Mon. Wea. Rev.*, **114,** 178–207.

Farrel, B. F., 1984: Modal and nonmodal baroclinic waves. *J. Atmos. Sci.*, **41,** 668–673.

Frederiksen, J. S., 1983: Disturbances and eddy fluxes in Northern Hemisphere flows: Instability of three-dimensional January and July flows. *J. Atmos. Sci.*, **40,** 836–855.

Held, I. M., 1985: Pseudomomentum and orthogonality of modes in shear flows. *J. Atmos. Sci.*, **42,** 2280–2288.

Hoskins, B. J., and T. Ambrizzi, 1993: Rossby wave propagation on a realistic longitudinally varying flow. *J. Atmos. Sci.*, **50,** 1661–1671.

Karoly, D. J., 1983: Rossby wave propagation in a barotropic atmosphere. *Dyn. Atmos. Oceans,* **7,** 111–125.

Lau, N.-C., 1988: Variability of the observed midlatitude storm tracks in relation to low-frequency changes in the circulation pattern. *J. Atmos. Sci.*, **45,** 2718–2743.

Lee, S., 1995: Localized storm tracks in the absence of local instability. *J. Atmos. Sci.*, **52,** 977–989.

——, and I. M. Held, 1993: Baroclinic wave packets in models and observations. *J. Atmos. Sci.*, **50,** 1413–1428.

Lim, G. H., and J. M. Wallace, 1991: Structure and evolution of baroclinic waves as inferred from regression. *J. Atmos. Sci.*, **48,** 1718–1732.

Nakamura, H., 1992: Midwinter suppression of baroclinic wave activity in the Pacific. *J. Atmos. Sci.*, **49,** 1629–1642.

Pierrehumbert, R. T., 1984: Local and global baroclinic instability of zonally varying flow. *J. Atmos. Sci.*, **41,** 2141–2162.

Plumb, R. A., 1986: Three-dimensional propagation of transient quasi-geostrophic eddies and its relationship with the eddy forcing of the time-mean flow. *J. Atmos. Sci.*, **43,** 1657–1678.

Simmons, A. J., J. M. Wallace, and G. W. Branstator, 1983: Barotropic wave propagation and instability, and atmospheric teleconnection patterns. *J. Atmos. Sci.*, **40,** 1363–1392.

Whitaker, J. S., and R. M. Dole, 1995: Organization of storm tracks in zonally varying flows. *J. Atmos. Sci.*, **52,** 1178–1191.